A Variable-Depth Green's Function for Shelf Edge Tides

CHRISTOPHER GARRETT AND BECHARA TOULANY

Department of Oceanography, Dalhousie University, Halifax, Nova Scotia, Canada B3H 4J1

(Manuscript received 15 May 1979, in final form 6 August 1979)

ABSTRACT

The Green's function for a semi-infinite ocean with depth a function of distance from the boundary is developed numerically for the M_2 frequency and with Coriolis frequency and depth profile appropriate to the continental slope off the Gulf of Maine. This involves numerical integration of the linearized shallow water equations for all longshore wavenumbers, followed by numerical Fourier transformation. This variable-depth Green's function is approximately equal to Buchwald's (1971) constant-depth Green's function for distances along the boundary greater than the width of the slope, and at very short range tends to limiting values which can be approximated analytically.

The Green's function, when combined with currents from Greenberg's (1979) numerical model of the Bay of Fundy and Gulf of Maine, is used to explain substantial observed variations in M_2 amplitude and phase along the edge of the shelf off the Gulf of Maine; the variable-depth Green's function produces significantly better results than the constant-depth Green's function. The results support the basic premise that the M_2 elevation at the shelf edge in the absence of the Gulf of Maine would be fairly constant, and suggest ways of deriving open boundary input for tidal models of coastal seas with a minimum of offshore gaging.

1. Introduction

The need to understand tidal currents and storm surges in coastal seas, and to predict changes in tidal regime that would be caused by large engineering developments, has led to increased numerical modeling of tides on the continental shelf (e.g., Flather, 1976; Choi, 1978; Greenberg, 1979). The shelf break forms a natural outer boundary for such models and, indeed, the use of models to predict changes in tidal regime requires that the open boundary be taken at the edge of the shelf to minimize the changes in the input (Garrett, 1975; Garrett and Greenberg, 1977).

The requirement for open boundary input data for the numerical models has, in turn, led to increased deployment of tide gages at the shelf break (e.g., Cartwright, 1976; DeWolfe, 1977). The considerable variability in tidal amplitude and phase along the shelf break, on a smaller scale than one would expect for deep-ocean tides, calls for explanation, and also raises the problem of deciding on an adequate density of gaging.

The calculations to be reported in this paper were motivated by an offshore gaging program, conducted off the Gulf of Maine in the summer of 1976 by David DeWolfe of Bedford Institute of Oceanography, that provided input data for Greenberg's (1979) numerical model. These studies were aimed at predicting the impact of potential tidal power development in the Bay of Fundy (both the gaging and the later stages of the numerical modeling being funded through the Bay of Fundy Tidal Power Review Board).

The locations of the seven successful deployments of tide gages (Aanderaa TG2A and TG3A) at the edge of the shelf are shown in Fig. 1 in relation to the grid used in Greenberg's (1979) numerical model. Details are given in Table 1. Three other tide gages were lost near boundary squares 3, 4 and 22. Eight successful deployments elsewhere in the Bay of Fundy and Gulf of Maine (DeWolfe, 1977) provided further verification data for Greenberg's (1979) model, but are not directly relevant to the present study. Only the amplitude and phase of the dominant tide (M_2) are given in Table 1, although harmonic constants for many other constituents were obtained (DeWolfe, 1977) and were, in fact, used in 29-day runs of Greenberg's (1979) model. As shown in Fig. 1, the tide gages were not all at the precise points for which input was required for Greenberg's (1979) model; the tidal data were used as input in the nearest boundary square, listed in Table 1. The listed phase lag is the Greenwich phase lag corrected for time zone GMT − 4.

The remarkable feature of the data is the substantial variation in M_2 phase, particularly in the vicinity of squares 20, 21, 22 at the mouth of the Fundian Channel. The increased phase lag in this important region, where much of the tidal mass flux into the Gulf of Maine occurs, was, in fact, contrary to a

0022-3670/79/061258-15$07.75

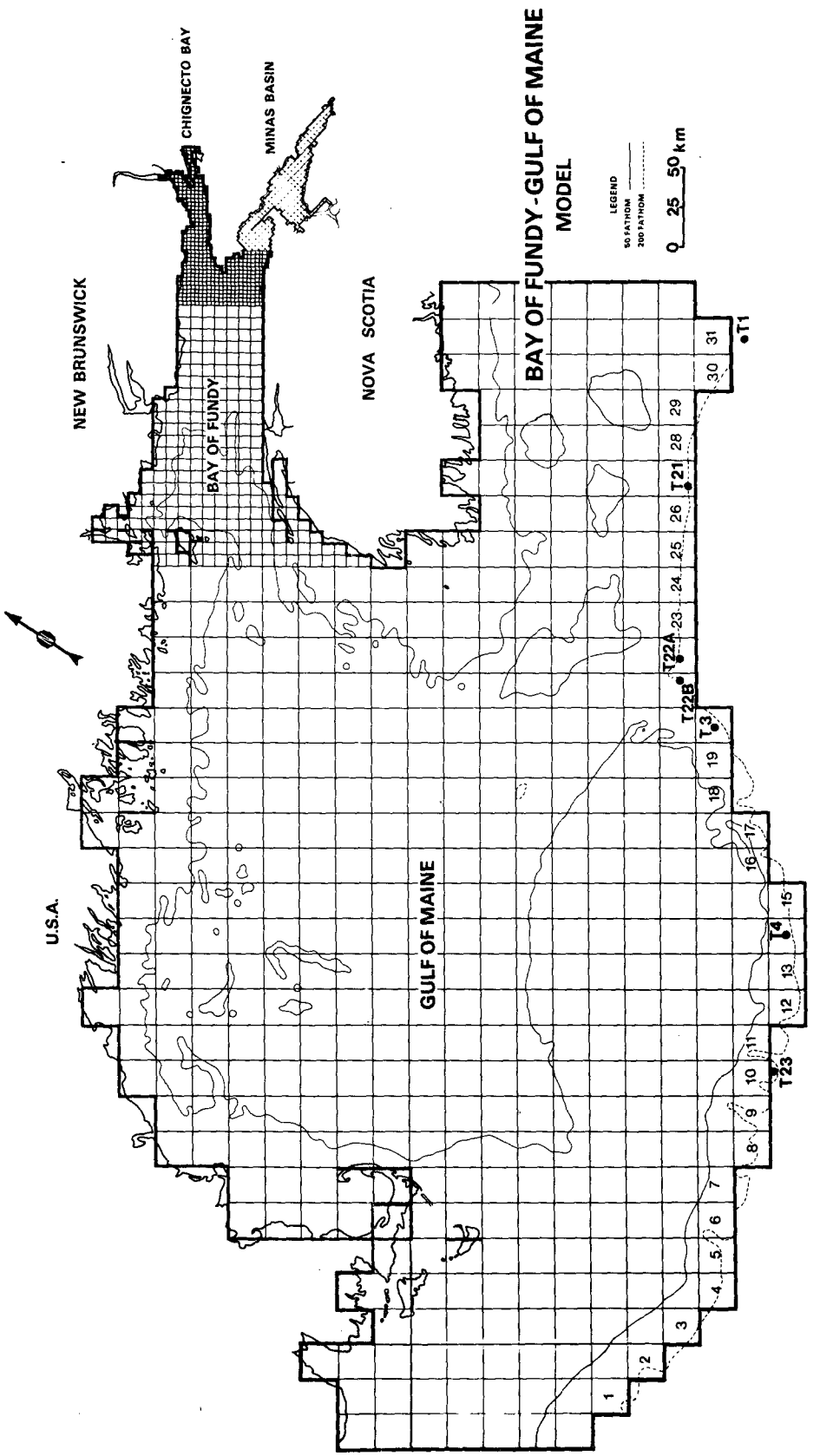

FIG. 1. Location of tide gages (prefix T) in relation to the grid of Greenberg's (1979) numerical model, for which M_2 elevation and phase are prescribed at the center of the outermost squares. At the shelf break these boundary squares are numbered from 1 to 31.

TABLE 1. Details of 1976 shelf edge tide gage program.

Gage No.	T23	T4	T3	T22B	T22A	T21	T1
Input square (see Fig. 1)	10	14	20	21	22	27	31
Latitude (°N)	40°22.1′	40°44.4′	41°44.3′	42°03.0′	42°07.1′	42°37.1′	42°49.0′
Longitude (°W)	67°45.0′	66°50.6′	65°48.1′	65°38.0′	65°30.1′	64°22.5′	63°12.8′
Water depth (m)	174	180	138	242	256	232	226
Date laid (1976)	12 Aug.	19 May	18 May	11 Aug.	11 Aug.	10 Aug.	18 May
Hours of record	1398	879	2034	1400	1399	1405	1505
M_2 amplitude (m)	0.407	0.404	0.396	0.442	0.458	0.490	0.482
M_2 phase lag (deg)	240.1	239.2	246.1	253.2	248.4	241.2	234.6

decrease assumed in an earlier version of Greenberg's model, developed before offshore data were available. This decreased phase was required by the earlier model for correct reproduction of M_2 amplitude and phase at the coast. The offshore data thus necessitated a recalibration of the model, which was done mainly by increasing the depth of the Gulf of Maine by 1.5 m. This was within the errors associated with extracting average depths from hydrographic charts but illustrates the sensitivity at tidal frequencies of the Bay of Fundy/Gulf of Maine system.

The observed increased phase lag is consistent qualitatively with Garrett and Greenberg's (1977) analysis of the effect on the elevation of the large mass flux into the Gulf of Maine, assuming that without the Bay of Fundy/Gulf of Maine system the M_2 amplitude and phase would be relatively constant, or at any rate vary slowly, along the edge of the shelf. They related the local changes in M_2 elevation to the computed currents using the constant depth Green's function of Voit (1958) and Buchwald (1971), assuming that from the edge of the shelf, assumed straight, the depth increased abruptly to a constant, and that the exterior ocean was semi-infinite. (They also discussed the excitation of near-resonant normal modes of the whole ocean, but these are assumed to have a large scale and not to contribute to the small-scale variations observed.) If one subtracts from the tide gage data the contribution associated with the mass flux across the shelf, using the Green's function for a semi-infinite ocean of depth 5000 m, the variation along the edge of the shelf is substantially reduced (Fig. 2). It was an averaged version of this result which formed the basis of Garrett and Greenberg's (1977) prediction of an increased phase lag in the vicinity of squares 20 to 22.

It is clear, though, that the correction in Fig. 2 does not go far enough. The data points still form a fairly large loop in the complex plane, possibly because of the inadequacy of a constant-depth Green's

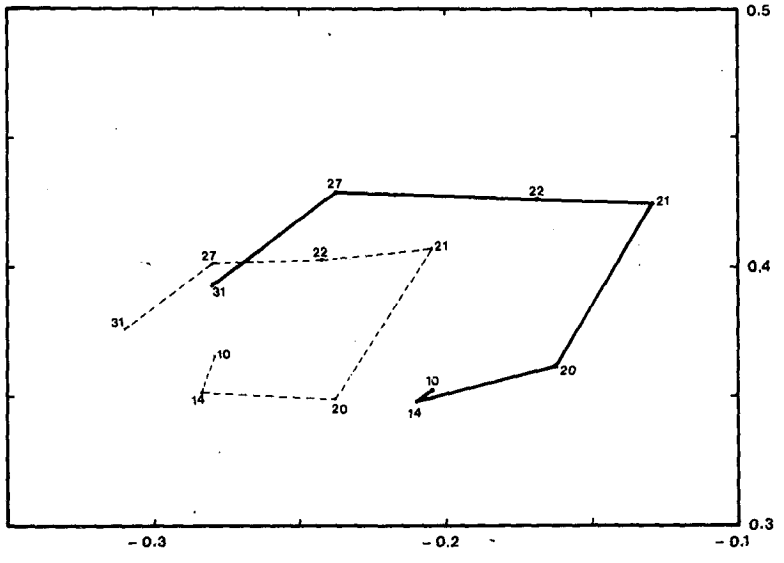

FIG. 2. Plot in the complex plane of points representing the amplitude and phase lead (=360° − phase lag) of M_2. Points connected by the solid lines correspond to the data from Table 1; points connected by the dashed lines have been corrected for the perturbation due to mass flux onto the shelf. Numbers denote the appropriate boundary square in Fig. 1.

function. The change in elevation, at a point on the edge of the shelf, due to a mass flux onto the shelf some distance away, may be largely due to the response of the deep ocean off the continental slope, but one would expect that the response to a local mass flux would depend strongly on the local depth and slope.

We thus decided to develop a Green's function which allows for the real topography of the continental slope (rather than assuming an abrupt drop to constant depth), while still assuming a straight shelf edge. Numerical development of this variable-depth Green's function, and application to the data set in question, forms the substance of this paper. Readers interested only in the application could turn to Section 11 via Figs. 5 and 6.

2. Separation of gulf and ocean

Fig. 3 shows a schematic of a continental shelf and gulf region, with a seaward mass flux Re $F(s)e^{i\omega t}$ across any position s on its boundary M. The elevation observed at any point s is Re $\zeta_M(s)e^{i\omega t}$, where

$$\zeta_M(s) = \zeta_0(s) - \int_M K_0(s,\sigma)F(\sigma)d\sigma. \qquad (2.1)$$

Here Re $\zeta_0(s)e^{i\omega t}$ is the elevation that would occur in the absence of a continental shelf (i.e., with zero mass flux across M), Re $F(\sigma)e^{i\omega t}$ is the mass flux (depth × current normal to M) at any position on M and $K_0(s,\sigma)$ is the elevation at s in response to unit shoreward mass flux (at frequency ω) across M at σ.

As discussed by Garrett and Greenberg (1977), $K_0(s,\sigma)$ can be expanded as an infinite series in terms of the normal modes of the exterior ocean. Any modes which are close to resonance at tidal frequencies will have a large scale compared with a typical coastal sea, and so will lead to a difference between ζ_M and ζ_0 that is fairly uniform over the boundary M in the vicinity of the gulf. Differences between ζ_M and ζ_0 on small spatial scales arise from the infinite tail of the normal mode expansion of $K_0(s,\sigma)$, which must behave like a local source and so look much the same as the Green's function for a semi-infinite ocean. We thus concentrate on deriving the Green's function for a semi-infinite ocean, and take the boundary M to be straight and the water depth a function of offshore distance only.

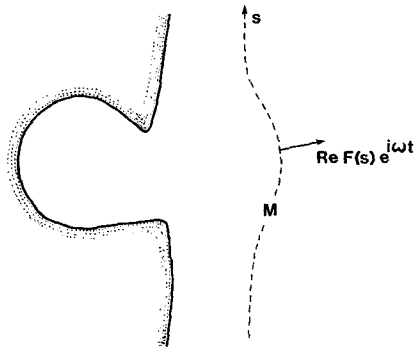

FIG. 3. Schematic of a continental shelf and gulf, separated from the deep ocean by the boundary M.

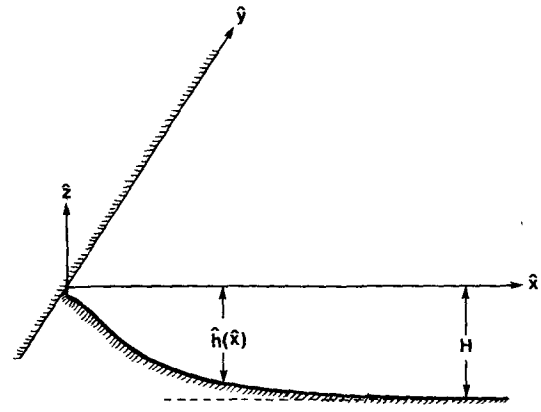

FIG. 4. Semi-infinite ocean with depth dependent on distance $\hat{x}$ from the boundary.

3. Variable-depth Green's function

We seek the elevation field that would be generated in the half-space $\hat{x} \geq 0$, and particularly on $\hat{x} = 0$, by an oscillating delta-function source at some point on the boundary $\hat{x} = 0$. The depth profile is $\hat{h}(\hat{x})$, with $\hat{h} \to H$ as $\hat{x} \to \infty$ (Fig. 4).

The current $(\hat{u},\hat{v})$ and elevation $\hat{\zeta}$, all assumed proportional to $\exp(i\hat{\omega}\hat{t})$, are governed by the linearized shallow water equations

$$i\hat{\omega}\hat{u} - f\hat{v} + g\partial\hat{\zeta}/\partial\hat{x} = 0, \qquad (3.1)$$

$$i\hat{\omega}\hat{v} + f\hat{u} + g\partial\hat{\zeta}/\partial\hat{y} = 0, \qquad (3.2)$$

$$i\hat{\omega}\hat{\zeta} + \hat{u}d\hat{h}/d\hat{x} + \hat{h}\partial\hat{u}/\partial\hat{x} + \hat{h}\partial\hat{v}/\partial\hat{y} = 0, \qquad (3.3)$$

where f and g are the Coriolis frequency and gravity. We nondimensionalize as follows:

$$\left.\begin{aligned} \hat{\omega} &= f\omega, \quad \hat{h} = Hh, \quad (\hat{u},\hat{v}) = U(u',v') \\ \hat{\zeta} &= (H/g)^{1/2}U\zeta', \quad (\hat{x},\hat{y}) = (gH/f^2)^{1/2}(x,y) \end{aligned}\right\}. \qquad (3.4)$$

We take the source at the origin to be

$$u'(0,y) = \delta(y) = (2\pi)^{-1}\int_{-\infty}^{\infty} \exp(-i\beta y)d\beta, \qquad (3.5)$$

and express the corresponding ζ' (the Green's function) as

$$\zeta_G(x,y) = (2\pi)^{-1}\int_{-\infty}^{\infty} \zeta(x,\beta)\exp(-i\beta y)d\beta, \qquad (3.6)$$

where $\zeta(x,\beta)$ satisfies the equations

$$\partial\zeta/\partial x = -i\omega^{-1}(\omega^2 - 1)u + \beta\omega^{-1}\zeta, \quad (3.7)$$

$$\partial u/\partial x = -(\beta\omega^{-1} + h^{-1}dh/dx)u + i(\beta^2\omega^{-1} - \omega h^{-1})\zeta. \quad (3.8)$$

The boundary conditions are $u = 1$ at $x = 0$ and, as $x \to \infty$, u, ζ either correspond to an outward propagating wave or remain finite. In fact, as $x \to \infty$, $h \to 1$, so that the correct solutions are

$$\zeta, u \propto \exp(-ikx), \quad \zeta/u = (\omega^2 - 1)/(k\omega - i\beta),$$

where

$$\left.\begin{aligned} k &= (\omega^2 - 1 - \beta^2)^{1/2}, \text{ for } |\beta| \leqslant (\omega^2 - 1)^{1/2} \\ \zeta, u &\propto \exp(-lx), \quad \zeta/u = i(\omega^2 - 1)/(l\omega + \beta) \end{aligned}\right\}, \quad (3.9)$$

where

$$l = (\beta^2 + 1 - \omega^2)^{1/2}, \text{ for } |\beta| \geqslant (\omega^2 - 1)^{1/2}. \quad (3.10)$$

If $h = 1$ everywhere these solutions apply for all x and lead to the constant-depth Green's function of Buchwald (1971). However, for a general $h(x)$ Eqs. (3.7) and (3.8) must be integrated numerically, and the Fourier transform (3.6) of the solution must also be evaluated numerically to determine the Green's function.

For a semi-infinite ocean with depth independent of the longshore coordinate, the kernel $K_0(s,\sigma)$ of (2.1) is related to the dimensionless Green's function by

$$K_0(s,\sigma) = -f[g\hat{h}(0)]^{-1} \times \zeta_G\,[0, f(gH)^{-1/2}(s - \sigma)]. \quad (3.11)$$

4. Depth profile

Fig. 5 shows the depth profile adopted for our calculations. It is based on a rough average of 12 sections (depth given by dots) across the part of the continental slope offshore from the Gulf of Maine (Fig. 6), with the origin at the 200 m isobath and the sections normal to it. We take the depth H for large $\hat{x}$ as 5 km which gives a length scale $(gH)^{1/2}/f$ of 2300 km for $f = 0.966 \times 10^{-4}\ \mathrm{s}^{-1}$ and $g = 9.81\ \mathrm{m\,s}^{-2}$. The dimensionless depth at the origin is $h(0) = 200/5000 = 0.04$ and we take $h(x) = 1$ for $x \geqslant 0.15$.

The only remaining parameter in Eqs. (3.7) and (3.8) which needs to be specified is the frequency. With $\hat{\omega} = 1.405 \times 10^{-4}\ \mathrm{s}^{-1}$ for M_2, we have $\omega = \hat{\omega}/f = 1.454$.

5. Numerical integration

We now solve (3.7) and (3.8) for different values of β, starting at $x = 0.2$ (greater than the value 0.15 beyond which $h = 1$) with the far-field solutions [(3.9) and (3.10)] of some arbitrary amplitude, and integrating back to the origin. We used the IMSL subroutine DVERK that employs Runge-Kutta formulas of orders 5 and 6, and gives significantly better results for large β than lower order schemes. The solution is normalized by division by $u(0,\beta)$ so as to satisfy the boundary condition $u(0,\beta) = 1$. In fact, if we are only interested in $\zeta_G(0,y)$, we only need $\zeta(0,\beta)$ which may be obtained as $F(0,\beta)$, where $F(x,\beta) = \zeta/u$ satisfies the single (but nonlinear), first-order ordinary differential equation

$$dF/dx = -i(\omega^2 - 1)/\omega + (2\beta\omega^{-1} + h^{-1}dh/dx)F - i(\beta^2\omega^{-1} - \omega h^{-1})F^2. \quad (5.1)$$

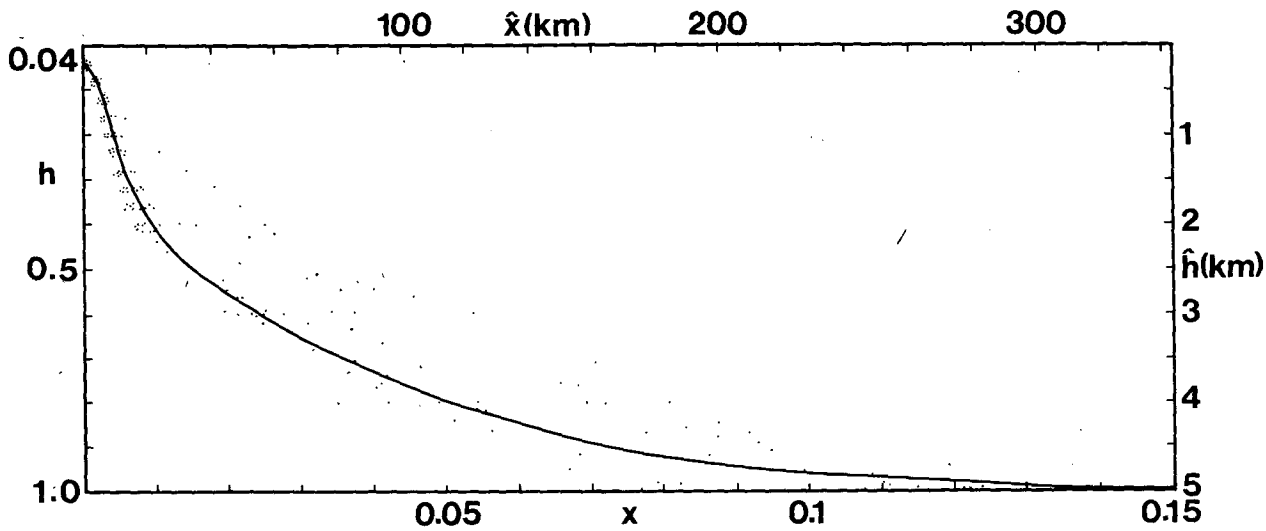

FIG. 5. Depth profile adopted, based on data (dots) from 12 sections across the continental slope shown in Fig. 6.

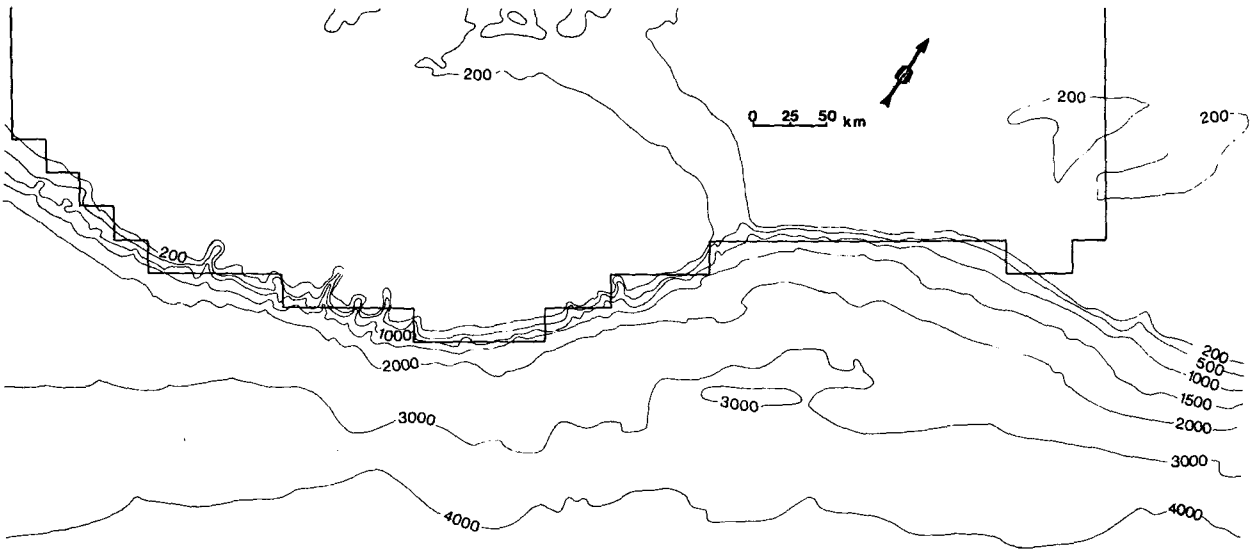

FIG. 6. Depth (m) offshore from the outer boundary (bold line) of the model region shown in Fig. 1.

In practice there was little difference in speed between solving (5.1) or (3.7) and (3.8) to five significant figures, so we used (3.7) and (3.8).

Fig. 7 shows $\zeta(0,\beta)$ for our $h(x)$. In fact we have multiplied our solution by 25 [the ratio $1/h(0)$] so as to normalize the forcing mass flux for comparison with $\zeta(0,\beta)$ for $h = 1$. Fig. 7 also shows $\zeta(0,\beta)$ for $h = 0.04$. The values of $\zeta(0,\beta)$ for constant depth are given by

$$\zeta(0,\beta) = \begin{cases} (\omega^2 - 1)/[(\beta_c^2 - \beta^2)^{1/2}\omega - i\beta], & |\beta| \leq \beta_c, \quad (5.2) \\ i(\omega^2 - 1)/[(\beta^2 - \beta_c^2)^{1/2}\omega + \beta], & |\beta| \geq \beta_c, \quad (5.3) \end{cases}$$

where

$$\beta_c = [(\omega^2 - 1)/h]^{1/2}. \quad (5.4)$$

The value of β_c is 1.056 for $h = 1$ and 5.278 for $h = 0.04$. For variable depth tending to 1 for large x we define β_c to be the same as for $h = 1$. It is the value of $|\beta|$ at which $\zeta(0,\beta)$ changes from complex to pure imaginary.

Fig. 7 shows that for small β, $25\zeta(0,\beta)$ for our variable depth profile is close to $\zeta(0,\beta)$ for $h = 1$. This is as expected; for long waves the elevation field is not sensitive to the reduction in depth for small x except that the driving mass flux, and hence the magnitude of the elevation field, is reduced by the ratio 0.04 of depths at the origin.

Fig. 7b shows that there is a singularity in $\zeta(0,\beta)$ at a negative value of β. For variable depth we have evaluated the precise position β_s of the singularity by determining the zero of $1/\zeta(0,\beta)$, and obtain $\beta_s = -1.496$. The shape of $-i/\zeta(0,\beta)$ (Fig. 8) indicates that, in the neighborhood of β_s, $\zeta(0,\beta)$ behaves like $iA/(\beta - \beta_s)$, and our computations of $\zeta(0,\beta)$ imply $A = -0.0447$.

It is convenient to separate out the singularity from $\zeta(0,\beta)$ by writing

$$\zeta(0,\beta) = G(\beta) + iA(\beta - \beta_s)^{-1}, \quad (5.5)$$

where $G(\beta)$ is now a smooth, finite function of β (Fig. 9). For constant depth $\beta_s = -\omega h^{-1/2}$, $A = -1$ and

$$G(\beta) = \begin{cases} [\omega(\beta_c^2 - \beta^2)^{1/2} - i\beta_s]/(\beta_s^2 - \beta^2), & |\beta| \leq \beta_c, \quad (5.6) \\ -i[\omega(\beta^2 - \beta_c^2)^{1/2} + \beta_s]/(\beta_s^2 - \beta^2), & |\beta| \geq \beta_c. \quad (5.7) \end{cases}$$

This has $G(\beta_s) = \frac{1}{2}i\omega h^{1/2}$, and we note that $G(\beta) = G(-\beta)$ for constant depth but not for variable depth.

Near β_s the value of $G(\beta)$ derived from (5.5) is very sensitive to the precision with which β_s, A and $\zeta(0,\beta)$ are computed. Our values of β_s, A are accurate to four significant figures, but we have still had to smooth $G(\beta)$ across β_s between its values at $\beta_s \pm 0.1$.

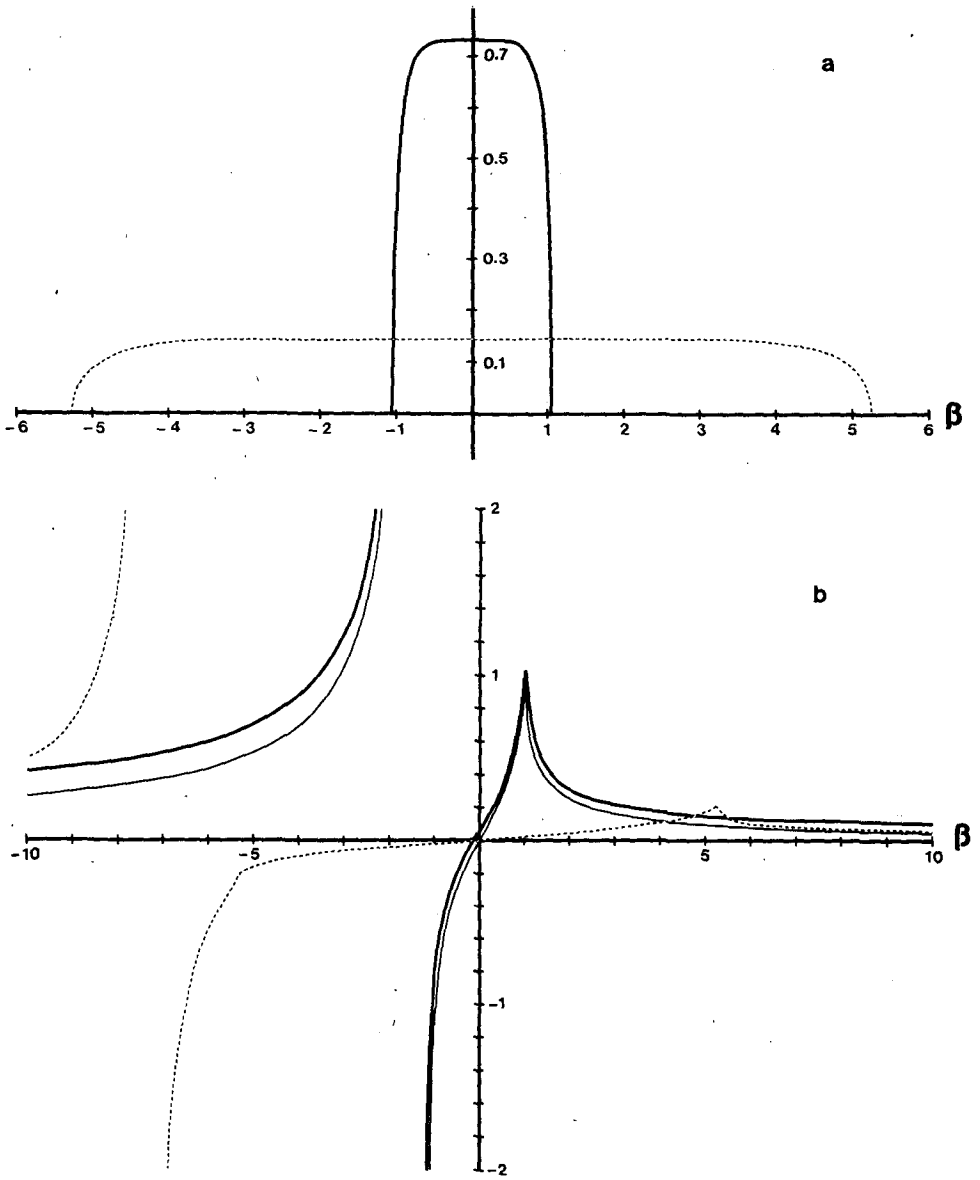

FIG. 7. $25\zeta(0,\beta)$ for our variable $h(x)$ (bold line), compared with $\zeta(0,\beta)$ for $h = 1$ (thin line) and for $h = 0.04$ (dashed line). (a) Real part, (b) imaginary part. The bold and solid lines are not separable in Fig. 7a.

6. Contribution of the singularity to the Green's function

The singularity at $\beta = \beta_s$ gives a contribution to the Green's function, on $x = 0$, denoted by

$$\zeta_s(0,y) = (2\pi)^{-1} \int_{-\infty}^{\infty} iA(\beta - \beta_s)^{-1} \exp(-i\beta y)d\beta. \quad (6.1)$$

To evaluate this we must choose a path of integration, around the pole at β_s, that is consistent with the radiation condition. For constant depth this is done by choosing $\omega = \omega' - i\epsilon$ (Buchwald, 1971), so that the solution is growing like $\exp(\epsilon t)$ and a wave decaying for large x corresponds to outward propagation. The singularity is then at $\beta_s = -\omega' h^{-1/2} + i\epsilon h^{-1/2}$ and the contour of integration in (6.1) passes below the pole, giving

$$\zeta_s(0,y) = \begin{cases} 0, & y \geq 0, \quad (6.2) \\ -A \exp(-i\beta_s y), & y < 0. \quad (6.3) \end{cases}$$

This is just a Kelvin wave propagating along the negative y axis and, since $\beta_s < 0$, clearly satisfies the condition of outward radiation.

For variable depth it is plausible, though difficult to prove, that writing $\omega = \omega' - i\epsilon$ moves β_s above

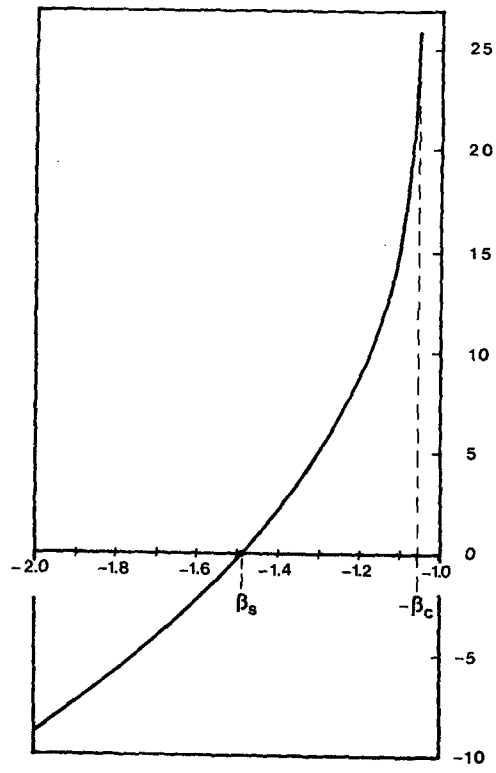

FIG. 8. $-i/\zeta(0,\beta)$ in the neighborhood of the singularity β_s of $\zeta(0,\beta)$ for variable depth.

the real axis. In any case, the requirement for the slightly modified Kelvin wave to propagate away from the source (assuming $|\beta_s|$ increases monotonically with ω to give a group velocity in the direction of β_s) leads to Eqs. (6.2) and (6.3) again as the contribution of the singularity to the Green's function.

7. Fourier transform of $G(\beta)$

It is convenient to write (3.6) at $x = 0$ as

$$\zeta_G(0,y) = \zeta_1 + \zeta_2 + \zeta_s, \tag{7.1}$$

where ζ_s is defined by (6.1) and ζ_1, ζ_2 by

$$\left.\begin{aligned} \zeta_1 &= (2\pi)^{-1}\int_{-\infty}^{\infty} \text{Re } G(\beta)\exp(-i\beta y)d\beta, \\ \zeta_2 &= (2\pi)^{-1}i\int_{-\infty}^{\infty} \text{Im } G(\beta)\exp(-i\beta y)d\beta \end{aligned}\right\}. \tag{7.2}$$

Here ζ_1 is easily evaluated numerically as Re $G(\beta) = 0$ for $|\beta| \geq \beta_c$, and we are only interested in values of $|y| \leq 0.3$, so that $\exp(-i\beta y)$ does not vary very rapidly. In fact, Re $G(\beta)$ for variable depth is almost exactly 0.04 times its value for $h = 1$, so that

$$\zeta_1 = 0.04\omega(2\pi)^{-1}\int_{-\beta_c}^{\beta_c} (\beta_c^2 - \beta^2)^{1/2} \times (\beta_s^2 - \beta^2)^{-1}\exp(-i\beta y)d\beta \tag{7.3}$$

$$= 0.02(\omega - 1) + O(|\beta_c y|^2) \tag{7.4}$$

Numerical evaluation of ζ_1 shows that the first term in (7.4) provides an accuracy of better than 2% for $|y| < 0.3$.

The contribution to ζ_2 from the integral of Im $G(\beta)\exp(-i\beta y)$ between $\pm\beta_c$ may be evaluated similarly. For $|\beta| > \beta_c$ the integrand, for either the sine or cosine integrals, consists of alternating lobes of decreasing magnitude. To evaluate the integrals

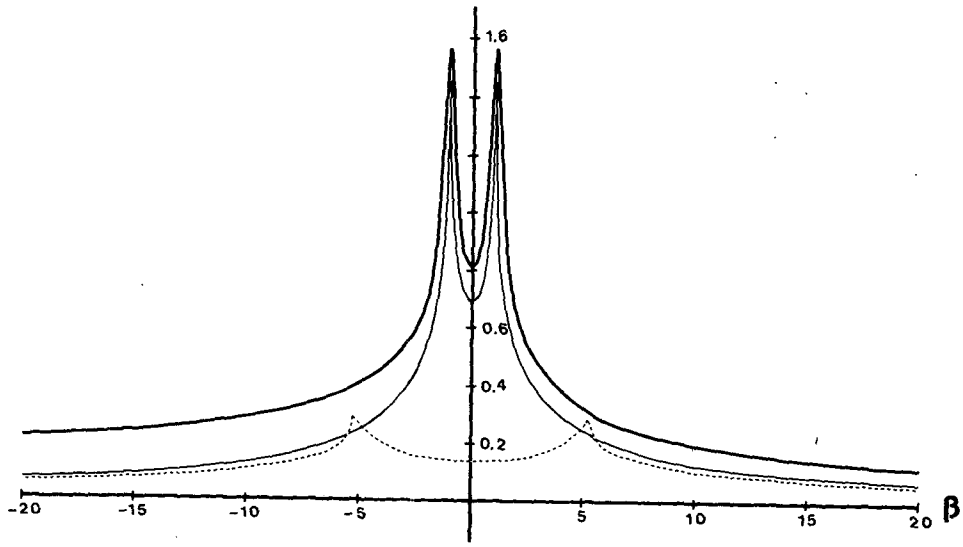

FIG. 9. 25Im $G(\beta)$ for variable depth (bold line), compared with Im $G(\beta)$ for $h = 1$ (thin line) and for $h = 0.04$ (dashed line).

numerically we used the subroutine TAIL, developed by R. L. Parker, which calls for numerical integration of the first 12 or so lobes, followed by repeated Euler transformation of the resulting series of terms of decreasing magnitude and alternating sign, followed by extrapolation to the sum of an infinite number of lobes. The process is rapid and accurate, with errors of less than a part in 10^5 for the values of $y \geq 10^{-2}$.

In carrying out this integration we need $G(\beta)$ or $\zeta(0,\beta)$, for $|\beta| > \beta_m = 3000$ or so, for which it can be obtained accurately from numerical integration of (3.7) and (3.8). For these large values of β we use the asymptotic form of $\zeta(0,\beta)$, valid for any depth profile,

$$\zeta(0,\beta) \sim i(\omega - 1)^{-1}, \quad G(\beta) = i(\omega - 1 - A)\beta^{-1} \quad \text{as} \quad \beta \to \infty, \tag{7.5}$$

$$\zeta(0,\beta) \sim -i(\omega + 1)^{-1}, \quad G(\beta) = -i(\omega + 1 + A)\beta^{-1} \quad \text{as} \quad \beta \to -\infty, \tag{7.6}$$

to which we add a term $C\beta^{-2}$ with the constant C, different for positive and negative β, chosen to ensure continuity of the computed and asymptotic forms at $\beta = \pm\beta_m$. The term $C\beta^{-2}$ only contributes 21% of Im $G(\beta)$ at $\beta = \beta_m$ and 24% at $\beta = -\beta_m$.

For very small values of $|y|$ ($<10^{-3}$ or so), it is convenient to evaluate the contribution to ζ_2 from $|\beta| > \beta_m$ in terms of the sine and cosine integrals Si ($|\beta_m y|$) and Ci ($|\beta_m y|$), rather than use TAIL.

The final result for $\zeta_G(0,y)$ is shown in Fig. 10.

8. Asymptotics

For $|\beta_c y| \ll 1$, the asymptotic form for $\zeta_G(0,y)$ for constant depth (Buchwald, 1971) is

$$\zeta_G(0,y) \sim \tfrac{1}{2}\omega\{1 - 2i\pi^{-1}[\ln(\tfrac{1}{2}\beta_c|y|) + \gamma]\} + (2\pi i)^{-1}\ln[(\omega + 1)/(\omega - 1)] - \tfrac{1}{2}(1 + i\beta_s|y|) \times \operatorname{sgn}(y) + O((\beta_c y)^2 \ln|\beta_c y|). \tag{8.1}$$

The comparison of this with the exact value for $h = 1$ (Fig. 10) confirms our integration and indicates the range of validity of (8.1).

9. The Green's function

Fig. 10 shows that, as one might expect, $25\zeta_G$ for variable depth is not greatly different from ζ_G for $h = 1$ except for $|y|$ less than a value comparable with the width of the continental slope (see Fig. 5). The computed value of Re $\zeta_G(0,y)$ as $y \to 0$ may be checked analytically. The contributions from ζ_s and ζ_1 are given by (6.3) and (7.4) and

$$\text{Re } \zeta_2(0,y) = (2\pi)^{-1}\int_{-\infty}^{\infty} \text{Im } G(\beta)\sin\beta y d\beta, \tag{9.1}$$

in which we may use the asymptotic forms (7.5) and (7.6) of Im $G(\beta)$ as $|y| \to 0$. Hence

$$\text{Re } \zeta_2(0,y) \to -\pi^{-1}(1 + A)\int_0^{\infty} \beta^{-1}\sin\beta y d\beta \tag{9.2}$$

$$= -\tfrac{1}{2}(1 + A)\operatorname{sgn} y, \tag{9.3}$$

so that as $|y| \to 0$

$$\text{Re } \zeta_G(0,y) \to \begin{cases} 0.02(\omega - 1) - \tfrac{1}{2}A - \tfrac{1}{2} = -0.4686, & y > 0, \\ 0.02(\omega - 1) - \tfrac{1}{2}A + \tfrac{1}{2} = 0.5314, & y < 0. \end{cases} \tag{9.4, 9.5}$$

For $h = 1$ the values are $\tfrac{1}{2}(\omega - 1)$ and $\tfrac{1}{2}(\omega + 1)$; for any depth profile Re ζ_G jumps by -1 across $y = 0$. For small $|y|$

$$\text{Im } \zeta_G(0,y) = (2\pi)^{-1} \times \int_{-\infty}^{\infty} \text{Im } G(\beta)\cos\beta y d\beta + O(|\beta_s y|). \tag{9.6}$$

From (7.5) and (7.6) this becomes $-\omega\pi^{-1}\ln|y|$ asymptotically as $y \to 0$, corresponding to source-like behavior in water of the local depth. In other words, Im $\zeta_G(0,y)$ for variable depth is asymptotically the same as Im $\zeta_G(0,y)$ for $h = 0.04$, given by (8.1). The difference plotted in Fig. 11, tends to a constant value as $y \to 0$, given by

$$(2\pi)^{-1}\int_{-\infty}^{\infty} (\text{Im } G|_{h=0.04} - \text{Im } G|_{\text{variable depth}})d\beta.$$

For our case this is numerically equal to 2.0.

Our computations are only for a particular value of ω and a particular choice of depth profile. However, the general behavior of ζ_G for a different ω and some other $h(x)$ representative of the continental slope can be established to some extent. For $|y|$ greater than a distance representative of the width of the slope ζ_G is $\sim h(0)$ times ζ_G for $h = 1$. For smaller $|y|$, Re ζ_G approaches $-\tfrac{1}{2}\omega h(0) - \tfrac{1}{2}$ for $y = \epsilon$ and $\tfrac{1}{2}\omega h(0) + \tfrac{1}{2}$ for $y = -\epsilon$ as $\epsilon \to 0$, with most of the change occurring very close to the origin. For small $|y|$ Im ζ_G for variable depth approaches Im ζ_G for constant depth $h(0)$ minus a constant, equal to 2.0 in our case, but with a dependence on ω and $h(x)$ which is not apparent without further work.

10. Discretization

In applying our Green's function to a situation in which the mass flux is given, not as a continuous

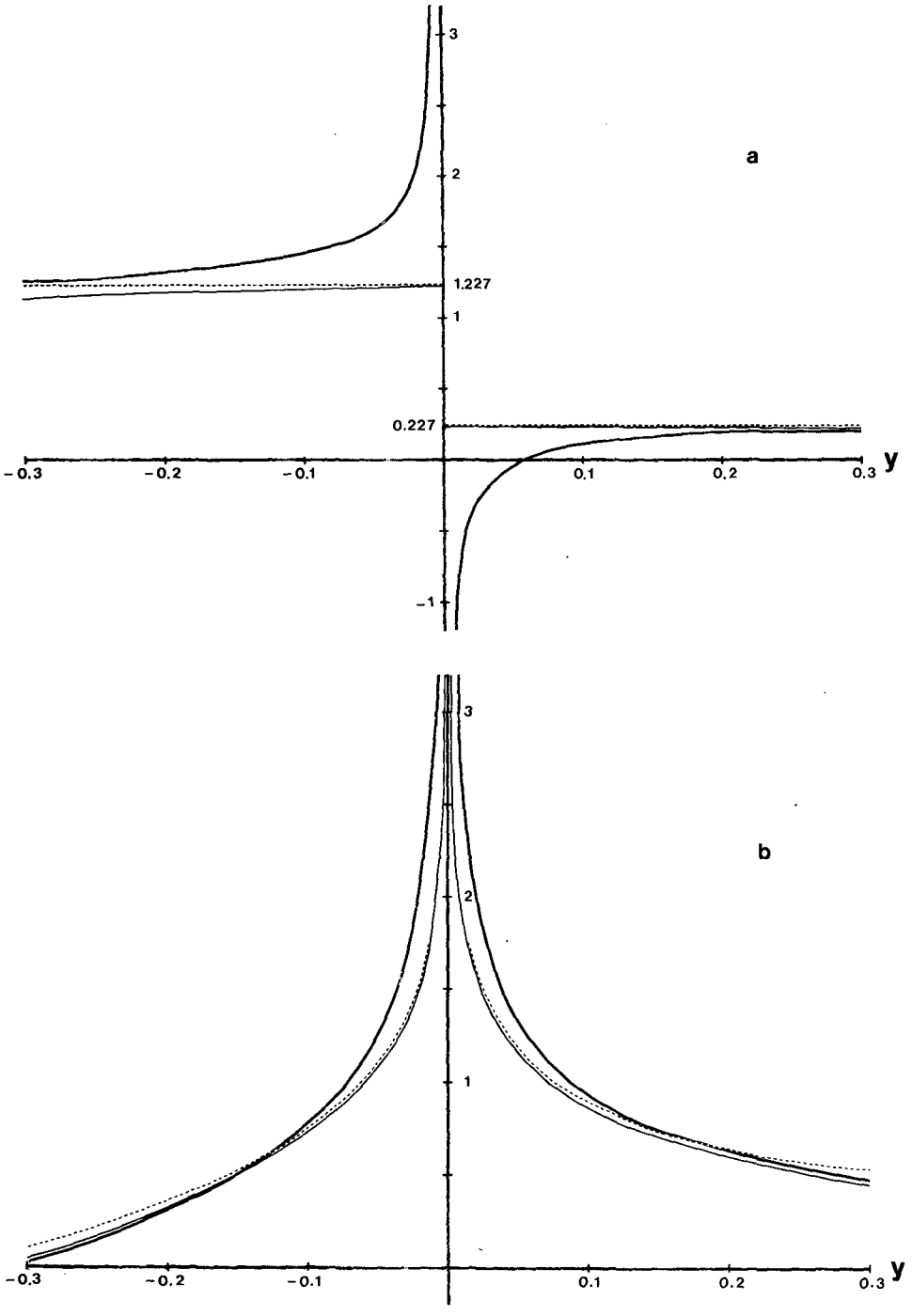

FIG. 10. $25\zeta_G(0,y)$ for variable depth (bold line), compared with $\zeta_G(0,y)$ for $h = 1$ (thin line). (a) Real part, (b) imaginary part. The dashed lines are the asymptotic form of $\zeta_G(0,y)$ for $h = 1$. As $y \to 0$, 25 Re $\zeta_G(0,y)$ for variable depth tends to 13.3 and -11.7 for positive and negative y, respectively, whereas Im $\zeta_G(0,y)$ is logarithmically singular.

function of y but as average values across the outer boundary of grid squares of finite size Δy, it is convenient to evaluate discrete values of ζ_G. We define

$$\zeta_{pq} = \zeta_G(0,(p-q)\Delta y), \quad p \neq q, \qquad (10.1)$$

as the average change in elevation in grid square p due to unit current across the boundary of square q. [An integral average from $(p-q-\frac{1}{2})\Delta y$ to $(p-q+\frac{1}{2})\Delta y$ would be more accurate, but the error is small for small Δy.]

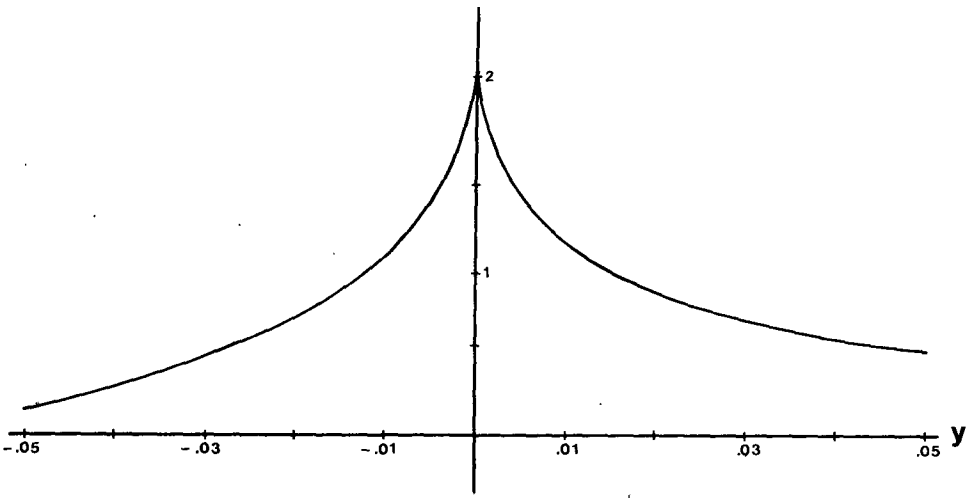

FIG. 11. Im $\zeta_G(0,y)$ for constant depth $h = 0.04$ − Im $\zeta_G(0,y)$ for variable depth.

For $p = q$, Eq. (10.1) breaks down and we must use the integral average, defining (Lee, 1971; Garrett and Greenberg, 1977)

$$\zeta_{pp} = (\Delta y)^{-1} \int_{-1/2\Delta y}^{1/2\Delta y} \zeta_G(0,y)dy. \qquad (10.2)$$

The integral is readily evaluated for constant depth using (8.1), but for variable depth there is no sufficiently accurate analytical approximation to $\zeta_G(0,y)$ for small y, and the singularity in $\zeta_G(0,y)$ makes numerical evaluation of (10.2) difficult. In this case we may write

$$\zeta_{pp} = (2\pi\Delta y)^{-1} \int_{-1/2\Delta y}^{1/2\Delta y} dy \int_{-\infty}^{\infty} d\beta G(\beta) \exp(-i\beta y) - A(\Delta y)^{-1} \int_{-1/2\Delta y}^{0} \exp(-i\beta_s y)dy, \qquad (10.3)$$

$$= (2\pi)^{-1} \int_{-\infty}^{\infty} G(\beta) \sin(\tfrac{1}{2}\beta\Delta y)/(\tfrac{1}{2}\beta\Delta y)d\beta + iA(\beta_s\Delta y)^{-1}[\exp(\tfrac{1}{2}i\beta_s\Delta y) - 1]. \qquad (10.4)$$

For our application $\Delta\hat{y} = 22.01$ km (ignoring slight variations due to the Mercator projection) so that the dimensionless $\Delta y = 9.57 \times 10^{-3}$. The integral (10.4) is evaluated in the manner described in Section 7. The resulting values of ζ_{pp} and ζ_{pq} are plotted in Fig. 12 as a function of p − q and compared with the values for $h = 1$. The major difference between $25\zeta_{pq}$ for variable depth and ζ_{pq} for constant depth occurs for small $p - q$, as expected, with particularly large changes in the imaginary part for $p = q$. However, we note that Im ζ_{pp} for variable depth, equal to 0.38, is still considerably less than the value 1.95 for $R = 0.04$ (the difference 1.57 can be checked from Fig. 11), and less than the value 2.0 for Σ Im ζ_{pq} for $p - q$ from −30 to +30 excluding zero. In other words, while the elevation change in one grid square in our application is particularly affected by the local current, the effect of more distant currents is likely to dominate.

11. Application

We now return to (2.1) and use our discretized Green's function to obtain an estimate, ζ_0, of the M_2 tide that would occur at the shelf edge off the Gulf of Maine, if the Gulf of Maine were closed off. First, we create 31-element arrays (Fig. 13) corresponding to the M_2 elevation ζ_{Mp} prescribed in Greenberg's (1979) model and to the resulting outward normal mass flux (current × depth) F_p along the open boundary of the model (see Fig. 2), derived from the numerical model. The elevation ζ_p corresponds to the tide gage data for $p = 10, 14, 20, 21, 22, 27, 31$, and to a smooth interpolation or extrapolation for other values of p. As in Garrett and Greenberg (1977), we include in F_p the mass flux, across any segment normal to the general trend of the shelf, that would enter the grid square with elevation ζ_p for the same value of p.

Having established ζ_{Mp} and F_p, we now compute

$$\zeta_{0p} = \zeta_{Mp} + \sum_{q=1}^{31} K_{pq}F_q\Delta\hat{y}; \qquad (11.1)$$

neglecting any M_2 mass flux onto the continental shelf that occurs on either side of the numerical

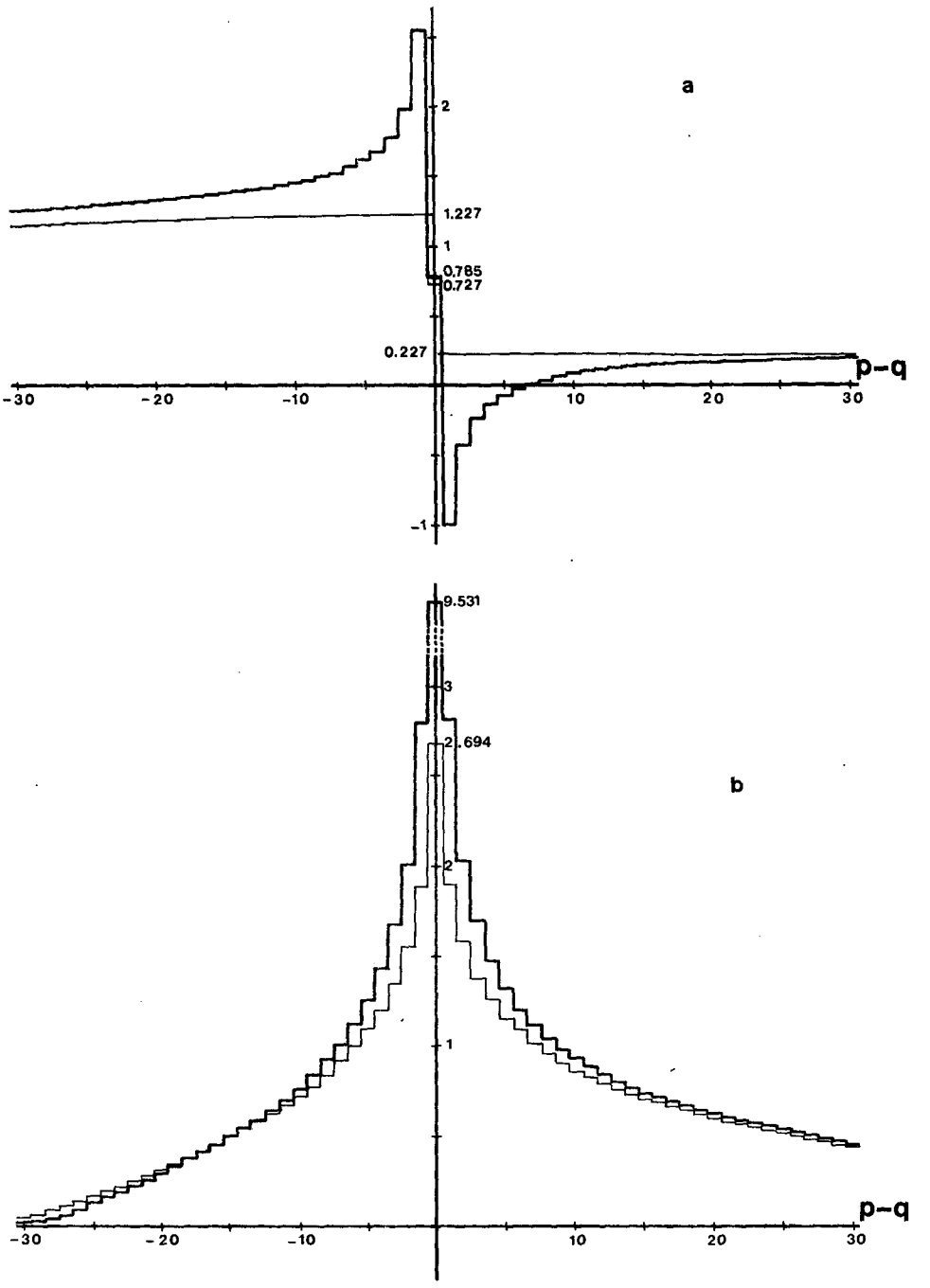

FIG. 12. $25\zeta_{pq}$ for variable depth (bold line) compared with ζ_{pq} for $h = 1$ (thin line). (a) Real part, (b) imaginary part.

model region shown in Fig. 2. In terms of our dimensionless Green's function matrix ζ_{pq},

$$K_{pq} = -25f\zeta_{pq}/gH \tag{11.2}$$

for variable depth and

$$K_{pq} = -f\zeta_{pq}/gH \tag{11.3}$$

for $h = 1$.

The resulting ζ_{0p}, for values of p corresponding to tide gage locations, is plotted in Fig. 14 for both the $h = 1$ Green's function (as in Fig. 2) and our variable-depth Green's function. We see that the latter produces a significantly tighter cluster of points. The reduced scatter and absence of any systematic trend suggests that ζ_{0p} in the absence of the

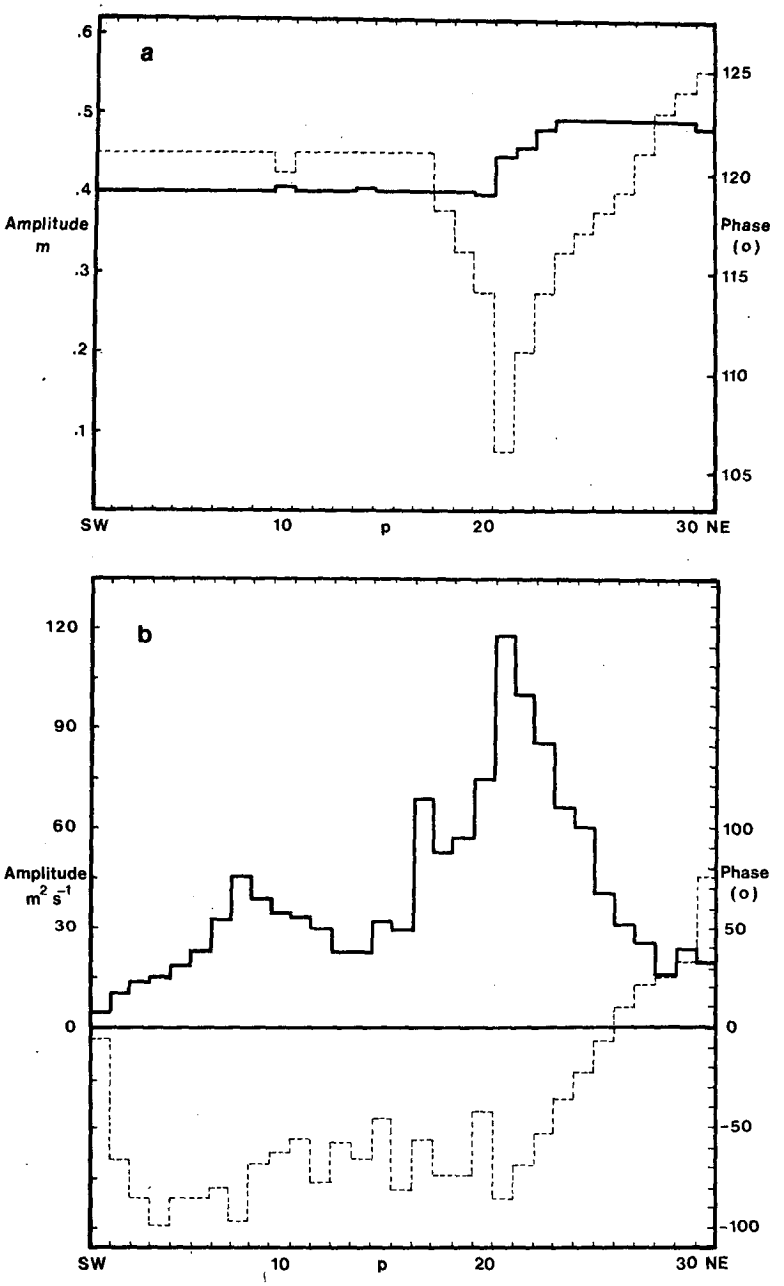

FIG. 13. Elevation ζ_M (a) prescribed at open boundary of model region (Fig. 1) and resulting seaward mass flux F across it (b). Amplitude (continuous line) and phase (dashed line).

Gulf of Maine would indeed be fairly constant along the edge of the shelf (as expected), with the remaining scatter in Fig. 14 due to lack of resolution of the model. In particular, we notice that the points with $p = 20, 21$ are associated with a corner region of the outer boundary in Fig. 1; an average of ζ_{0p} for 20 and 21 would lie closer to the rest of the points in Fig. 14.

Our predicted ζ_{0p}, in fact, is not quite what would be expected in the absence of the Gulf of Maine, as we have omitted from K_{pq} terms corresponding to near-resonant excitation of ocean normal modes that are relatively constant across the entrance to the Gulf of Maine. From the estimates of Garrett and Greenberg (1977) a contribution (0.057 m, $-111°$) arises from excitation of the 12.8 h North Atlantic mode by the mass flux into the Gulf of Maine, and this could be subtracted from all our estimates of ζ_{0p} in Fig. 14 to obtain the best estimate of ζ_0.

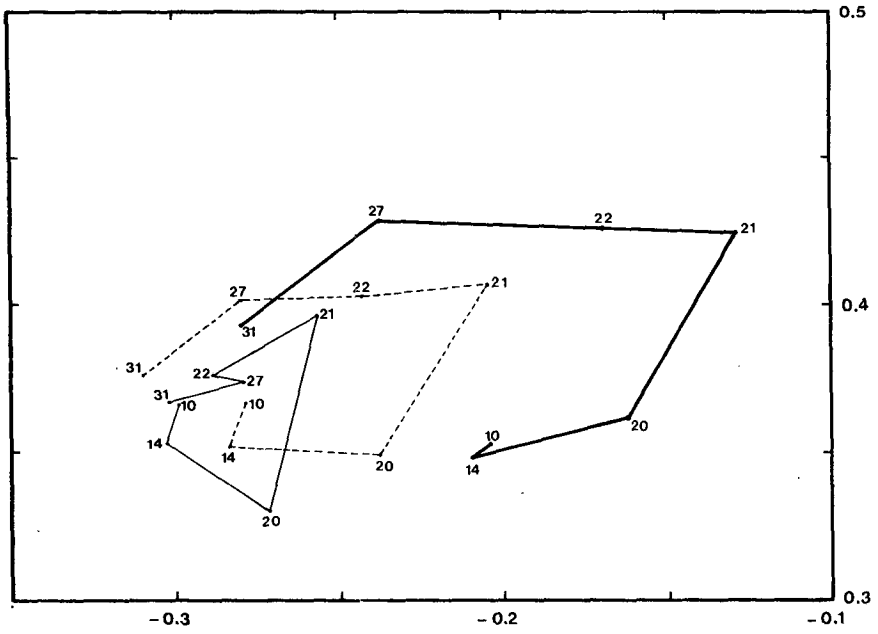

FIG. 14. M_2 elevation of tide gage locations: measured ζ_{Mp} (points joined by bold line), calculated ζ_{0p} using constant-depth Green's function (dashed line) and calculated ζ_{0p} using variable-depth Green's function (thin line).

Fig. 15 shows ζ_{0p} amplitude and phase for all p for our variable depth Green's function. Apart from small-scale variations which we presume are associated with poor resolution of our model, the only systematic trend is in the phase for small values of p. This suggests that in the southwestern section of the open boundary of the model (Fig. 1), where Greenberg (1979) assumed, in the absence of tide gage data, a constant phase lead of 121°, a phase of 126° at $p = 1$ decreasing to 120° at $p = 10$ would have been more suitable. Further gaging in this area would be most interesting.

12. Impedance

In predicting the changes in tidal regime in the Bay of Fundy/Gulf of Maine system that would be caused by tidal power development, Greenberg

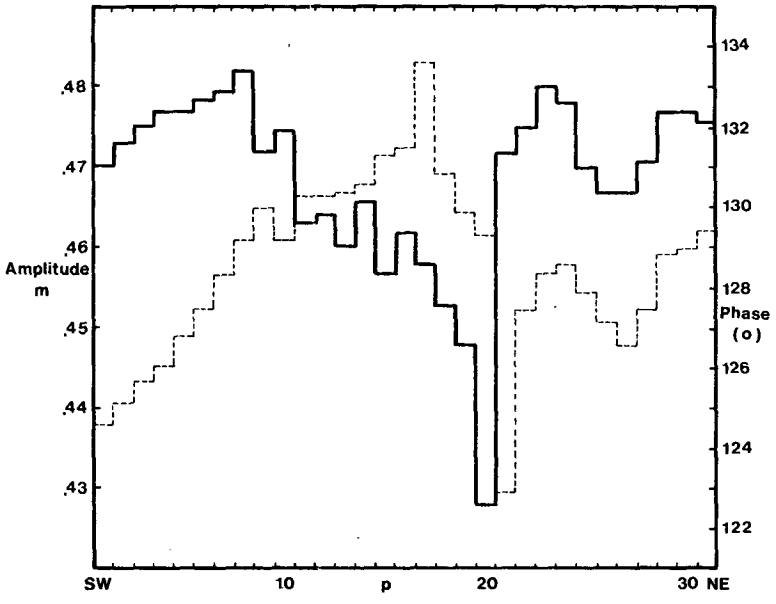

FIG. 15. Predicted elevation ζ_0 from Eq. (11.1). Amplitude (continuous line) and phase (dashed line).

(1979) made the conventional assumption that the input on the open boundary of the model (Fig. 1) would be unchanged. Garrett and Greenberg (1977) pointed out that this is incorrect and made estimates of the average change to be expected on the open boundary due to the finite impedance of the exterior ocean. These estimates of the ocean impedance were based on a constant-depth Green's function, and may now be revised using the more appropriate variable-depth Green's function developed in this paper. As expected, the ocean impedance increases in magnitude, from $(3.6 \times 10^{-9}\ m^{-2}\ s, -120°)$ to $(4.3 \times 10^{-9}\ m^{-2}\ s, -115°)$, implying slightly greater changes at the open boundary. Allowing also for excitation of the 12.8 h North Atlantic normal mode leads to predictions of correction factors 0.990 and 0.974 for M_2 for the Economy Point and Cape Blomidon plants considered by Garrett and Greenberg (1977), almost identical to their 0.991 and 0.974. In other words, Greenberg's (1979) predicted average M_2 increases of 4.8 and 16.6% are reduced to 3.8 and 13.6%, respectively. Our variable depth Green's function does not alter the semi-quantitative conclusion of Garrett and Greenberg (1975) that predicted changes in M_2 are uncertain to $\sim \pm 25\%$ of the change in M_2 mass flux across the shelf edge.

13. Discussion

We have used our variable depth Green's function, together with M_2 elevation ζ_M measured at the edge of the shelf and currents from a numerical model, to estimate what the elevation ζ_0 would be in the absence of a particular region of continental shelf. As expected, ζ_0 varies much less along the edge of the shelf than ζ_M. If this is a general result, the following possibilities are suggested:

1) If one had detailed measurements of ζ_M, could one assume a value of ζ_0 (constant along the edge of the shelf) and invert (2.1) or (11.1) to estimate the mass flux F? One suspects that small errors in ζ_M would lead to erratic estimates of F; direct measurements of the currents or, as here, derivation of the mass flux from a numerical model of the coastal region, would be much more reliable.

2) A more useful application of the theory of this paper would be to provide corrected input for a numerical model of the shelf and Gulf. One could start with an estimated ζ_M at the open boundary and calibrate the model (through minor adjustments of friction, coastline geometry and water depth) to reproduce the observed tides at the coast. This would give the mass flux across the open boundary, leading to an estimate of ζ_0 from (2.1) or (11.1). If this were not constant or were slowly varying along the open boundary, ζ_M could be adjusted appropriately and the process repeated, leading to very rapid convergence. Some ambiguity would remain, so that offshore gaging is always likely to be necessary, but the above scheme could be useful for interpolating between sparse observation or for extrapolating to positions further along the shelf, as in Section 11.

Acknowledgments. We thank Dave DeWolfe for permission to use and quote the results of his shelf edge tide measurements, Dave Greenberg for providing us with detailed results from his numerical model and Bob Reid for comments. The Natural Sciences and Engineering Research Council of Canada provided financial support.

REFERENCES

Buchwald, V. T., 1971: The diffraction of tides by a narrow channel. *J. Fluid Mech.*, **46,** 501–511.

Cartwright, D. E., 1976: Shelf boundary tidal measurements between Ireland and Norway. *Mém. Soc. Roy. Sci. Liège*, Ser. 6, **10,** 133–139.

Choi, B., 1978: Computation of barrier effects on tides in Inchon Bay. *Proc. Int. Symp. Korean Tidal Power*, Korean Ocean Res. Development Inst., Seoul, 325–340.

DeWolfe, D. L., 1977: Unpublished manuscript. Bedford Institute of Oceanography; and see Chap. 4 of Reassessment of Fundy Tidal Power, Minister of Supply and Services, Canada, 1977.

Flather, R. A., 1976: A tidal model of the northwest European continental shelf. *Mém. Soc. Roy. Sci. Liège*, Ser. 6, **10,** 141–164.

Garrett, C. J. R., 1975: Tides in gulfs. *Deep-Sea Res.*, **22,** 23–35.

——, and D. A. Greenberg, 1977: Predicting changes in tidal regime: The open boundary problem. *J. Phys. Oceanogr.*, **7,** 171–181.

Greenberg, D. A., 1979: A numerical model investigation of tidal phenomena in the Bay of Fundy and Gulf of Maine. *Mar. Geodesy*, **2,** 161–187.

Lee, J.-J., 1971: Wave-induced oscillations in harbours of arbitrary geometry. *J. Fluid Mech.*, **45,** 375–394.

Voit, S. S., 1958: The propagation of tidal waves from a strait into an ocean basin. *Izv. Akad. Nauk SSR Ser. Geofiz.*, **4,** 486–496.